

1 *In situ* monitoring of pit gas composition during baking of anodes for aluminum electrolysis

2
3 Trond Brandvik¹, Heiko Gaertner², Arne P. Ratvik², Tor Grande¹, Thor A. Aarhaug²

4
5 ¹Department of Materials Science and Engineering, NTNU Norwegian University of Science and
6 Technology, 7034 Trondheim, Norway

7 ²SINTEF Industry, 7465 Trondheim, Norway

8
9 Corresponding author: Thor Anders Aarhaug (thor.a.aarhaug@sintef.no)

10
11
12 **Abstract**

13 Carbon anodes, which are consumed in aluminum electrolysis, are fabricated in separate anode plants
14 where coke and pitch are mixed and vibrocompacted to green anode blocks before being baked in
15 anode baking furnaces. The chemical environment inside an anode baking furnace is found to play an
16 important role in the degradation of the furnace refractory lining. In this work, the pit gas composition
17 was recorded during anode baking by an FTIR spectrometer and a gas chromatograph. The
18 temperature dependence of the concentration of gas species during baking were obtained based on
19 three measurement campaigns., The concentrations of CO and CO₂ were found to be very dependent
20 on temperature, where the concentration of CO peaked around the maximum firing temperature. In
21 addition to varying concentrations of CH₄ and HF, water was found in large amounts in the first part
22 of the baking cycle. The water is to some extent originating from the cooling of the green anodes after
23 vibrocompaction and is potentially important with respect to the chemical stability of the refractory
24 lining. The variations in pit gas composition is related to operational parameters and discussed in
25 relation to refractory degradation phenomena.

26 **1. Introduction**

27 The most used anode technology in state-of-the-art aluminum electrolysis cells is prebaked carbon
28 anodes ^[1,2]. Anodes are manufactured in separate anode fabrication plants where the final step is the
29 anode baking. The green anodes consists of petroleum coke, anode butts and coal tar pitch which are
30 mixed and vibrocompacted to individual anode blocks prior to heat treatment (baking) in the anode
31 baking furnace ^[3]. Over the course of the lifetime of the furnace, the refractory lining are exposed to
32 both temperature cycling and gaseous reactions causing material changes in the refractory. Hence, the
33 walls are subjected to stress of physical, thermal and chemical nature, reflected in observed
34 degradation of the refractory walls ^[3-5]. Commonly, the walls are found to bend along the length of
35 the pit walls, which, together with carbon deposition, is decreasing the pit width and the space in

36 which the anodes are placed during baking. At some point, the pits become too narrow and the walls
37 must be replaced in order to fit the anodes into the pits [3-5].

38 Investigations of refractory degradation in anode baking furnaces have suggested several possible
39 mechanism for the material degradation [6-9]. The most widely discussed cause of degradation is
40 reactions with sodium and/or fluorine containing compounds. Investigations of spent lining from
41 industrial furnaces have revealed significant levels of sodium in the regions close to the anode pit
42 [4,5,9,10]. The level of amorphous phases is also found to be higher in these regions. Sodium, mostly
43 introduced through frozen bath from the anode butts, forms volatile compounds during heat treatment.
44 Both crystalline and amorphous sodium aluminosilicate phases have been observed in linings due to
45 chemical reactions involving sodium during baking[4,5,9]. However, in later studies, the sodium level in
46 the spent lining is not observed to be equally high, reducing the significance of sodium influence on
47 the refractory stability in some furnaces [8]. In addition to the reactions with volatile sodium fluorides,
48 the effect of reducing atmosphere on refractory stability has been discussed [9]. It is suggested that
49 reducing gaseous compounds (H₂, CH₄, CO etc.) could affect the stability of the oxides at elevated
50 temperatures, explaining some of the observations reported [9]. Detailed knowledge on pit gas
51 composition therefore of high interest, and could improve the understanding of degradation
52 mechanism of the lining. Investigations of pit gas atmosphere during anode baking has, to the best of
53 the authors knowledge, not been reported by others, and the pit gas composition as a function of time
54 and temperature during baking has been largely unknown. Preliminary studies conducted by the
55 authors have shown that the concept of *in situ* measurements of pit gas is feasible, although
56 challenging [11,12].

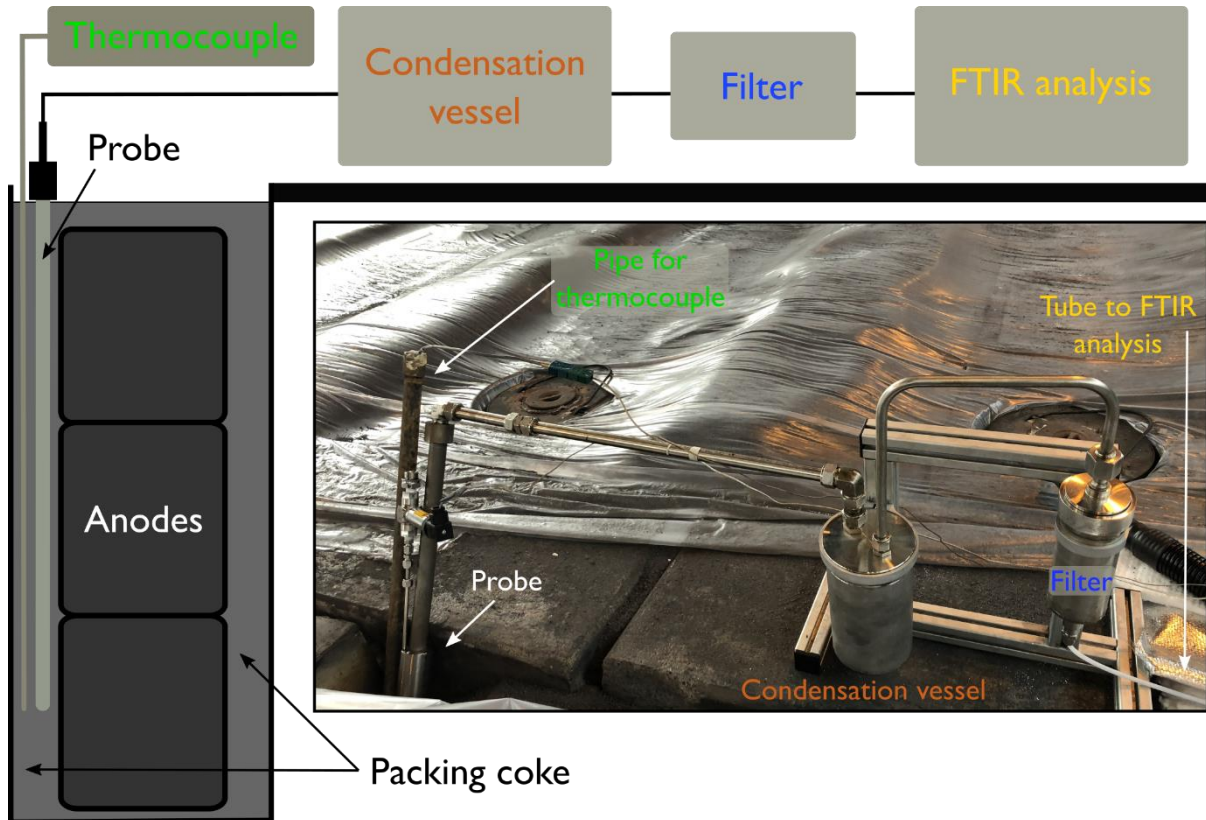
57 Here, we report on three measurement campaigns conducted in the same baking furnace. Based on the
58 experience from the initial study[11], the sampling setup was adjusted and improved in order to expand
59 the sampling period over the whole baking cycle. Pit gas composition as function of time and
60 temperature was measured by a Fourier transformed infrared spectroscopy (FTIR) as described by
61 Aarhaug *et al.* [11,12]. Composition of pit atmosphere, with especial focus on CO, CO₂, CH₄ and HF,
62 were investigated and related to operational conditions of the furnace and the degradation of the
63 refractory lining. Further modifications of the experimental setup were carried out before the last
64 measurement campaign. The outcome obtained from the setup modifications is finally discussed.

65 **2. Experimental**

66 **2.1 Experimental setup**

67 The anode gas measurements were conducted through three experimental series in an open anode
68 baking furnace. The initial experimental setup design consisted of a Kanthal (FeCrAl alloy) probe,
69 inserted into the pit through the packing coke. The probe was made of two concentrically mounted
70 Kanthal pipes with dimensions as shown in Figure 1. The double pipe construction was chosen for

71 increased mechanical support of the inner pipe in addition to reduce the risk of pipe blockage by
 72 packing coke. Above the packing coke, the two pipes were both mounted to a stainless steel (SS)
 73 connector, which on the top side where connected to the sampling line through a 1/4" SS connector.
 74 The first part of the sampling line consisted of a steel pipe (5 m, Ø 1/4"), before a 1/4"
 75 polytetrafluoreten (PTFE) tube surrounded by a heating tube (20 m, 180 °C) connected the probe to a
 76 cylindrical filter (Ø 10 cm, 30 cm length) filled with glass wool, and subsequently the FTIR in the
 77 end.



78
 79

80 Figure 1: Overview of the experimental setup used in the second and third measurement campaigns.
 81 The Kanthal probe consists of two concentrically mounted pipes. The inner diameter, outer diameter
 82 and length are 20.9 mm, 36.7 mm and 4200 mm (inner pipe), and 34 mm, 40 mm and 4500 mm (outer
 83 pipe), respectively. The probe inlet is in the bottom of the pit, measuring the gas composition
 84 approximately 1 meter above the pit floor.

85 Several parts of the experimental setup design were improved prior to the second and third series. A
 86 cylindrical condensation unit with an approximate volume of 2 litres was constructed, with gas inlet
 87 and outlet mounted in the lid. The setup used for the second and third series is presented in Figure 1.
 88 The cylinder and lid were connected with threads allowing the cylinder to be disconnected from the
 89 lid and its content removed. To avoid problems with condensation in the piping between the probe
 90 and the condensation unit, the pipe diameter was increased from 1/4" to 1/2" and 3/4" in this part of the
 91 setup. After the condensation unit, a filter unit was mounted to remove potential volatile polyaromatic

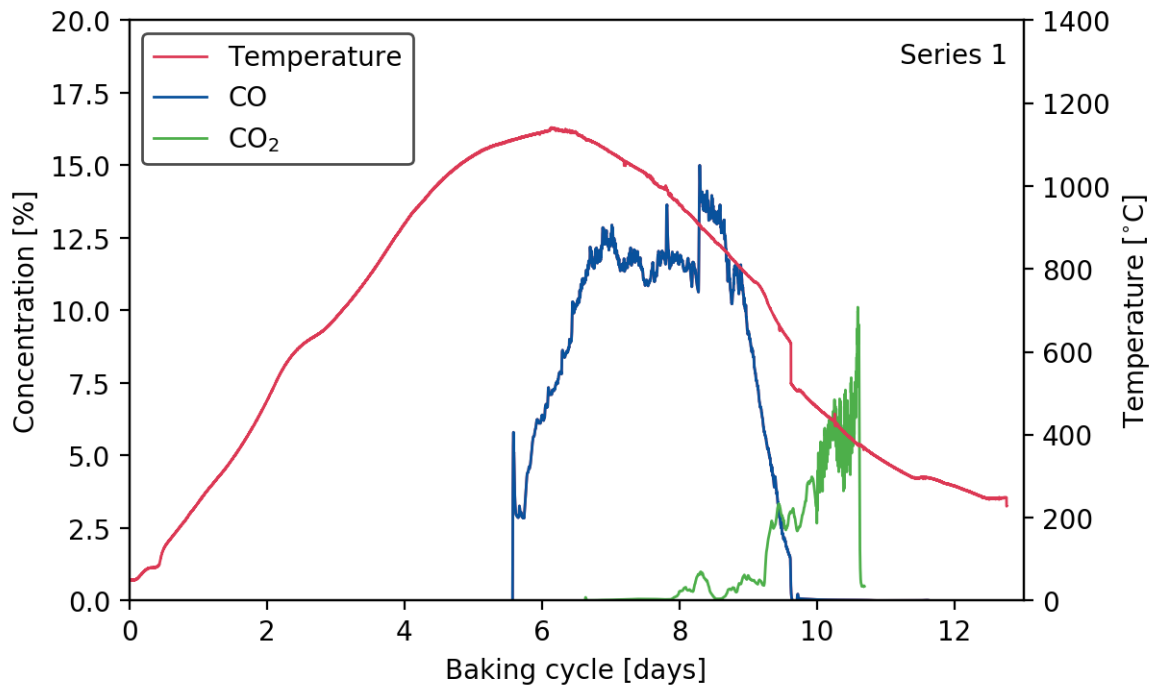
92 hydrocarbons (PAHs) in the gas flow. The filter unit consisted of an outer shell, with an inner
93 removable cylinder filled with XAD-2 adsorbent instead of the glass wool used as filter material in
94 the first series. The gas exited the filter unit and reached the FTIR instrument the same way as in the
95 first series. In the third series, the experiment was expanded to include a gas chromatograph
96 connected in series after the FTIR instrument. The probe was inserted into the pit between the anodes
97 and the flue wall prior to adding the packing coke, with the probe inlet positioned approximately in
98 the middle between both side walls and 1 meter above the pit floor. For all three series, a
99 thermocouple was inserted into the packing coke together with the Kanthal probe, measuring the
100 temperature by the probe inlet.

101 **2.2 Analysis**

102 The FTIR analysis was carried out with a Protea LTD ProtIR 204M analyser. The equipment recorded
103 data with a resolution of 1 cm^{-1} , averaging spectral data every 1-5 minutes. The instrument was heated
104 to $180\text{ }^{\circ}\text{C}$, the same temperature as the Teflon tube leading the gas from the filter unit to the
105 instrument. Library FTIR data of the expected gaseous species was used as basis for comparison
106 during manual interpretation of the spectral data. Linear regression of peak height values was used to
107 quantify the amount of each gas species. When spectral data from the experiments were outside the
108 range of the library data, extrapolation of library data was performed. The instrument's built-in
109 calibration model was in some cases applicable. An Agilent 490 Pro GC was calibrated for H_2 , O_2 , N_2
110 and CO_2 and was added to give information about the dilution of the air as well as oxygen
111 concentration in the pit.

112 **3. Results**

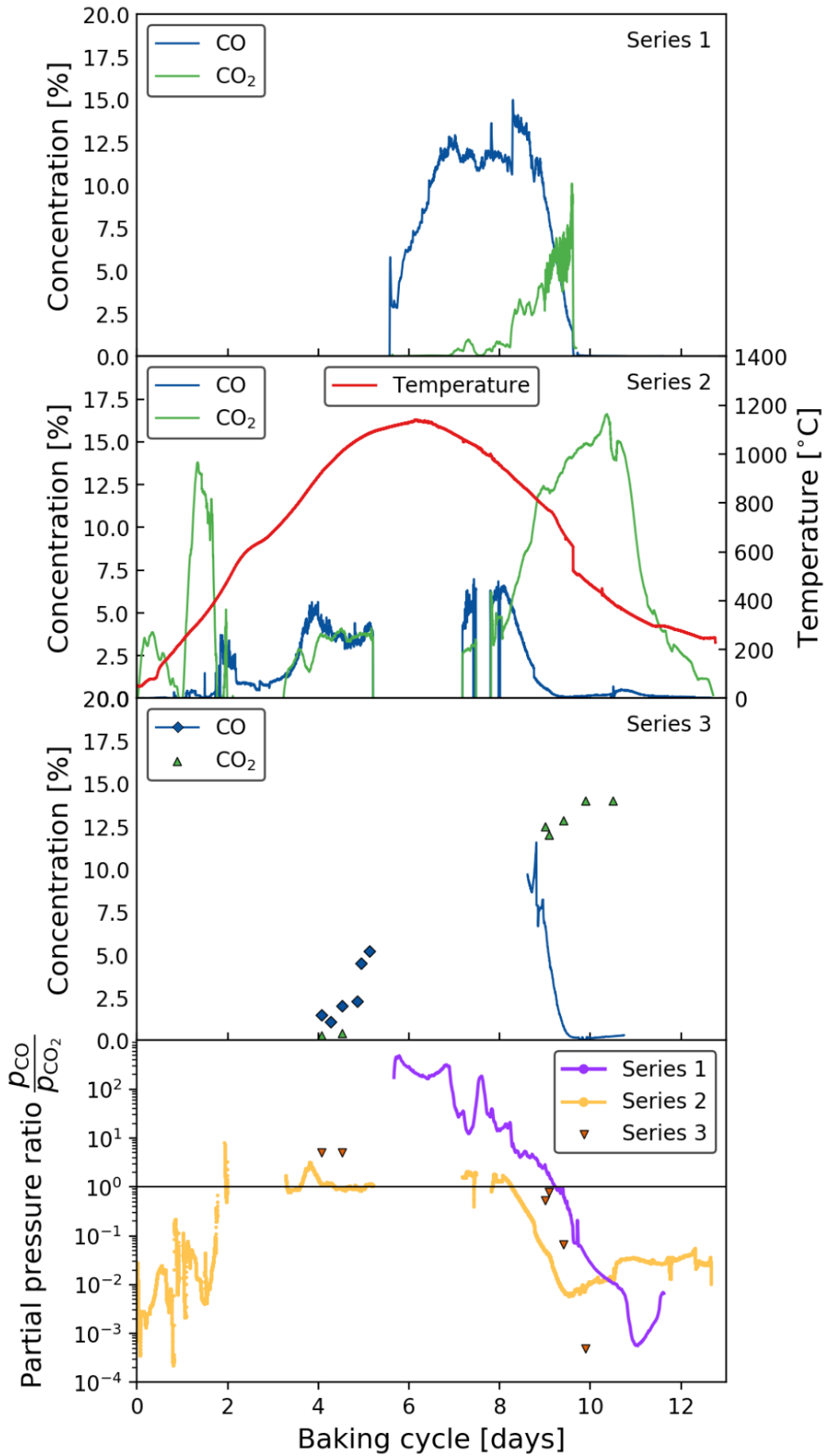
113 Concentrations of CO and CO_2 from series 1 are presented in Figure 2. Here, concentrations are
114 plotted as a function of time, i.e. days in the baking cycle. The figure shows a time span of 13 days,
115 which is a typical length of a baking cycle. The measured temperature is also shown, linking the
116 concentration of CO and CO_2 to the temperature and number of days into the baking cycle. The
117 maximum temperature measured in the packing coke is almost $1200\text{ }^{\circ}\text{C}$. The measurements of series 1
118 was initiated ~ 5.5 days into the cycle, in a period where CO is dominating over CO_2 in the pit gas. As
119 temperature decreases, the concentration of CO decreases while CO_2 increases. The data from series 1
120 was terminated at ~ 10.5 days, resulting in only partial coverage of the baking cycle.



121

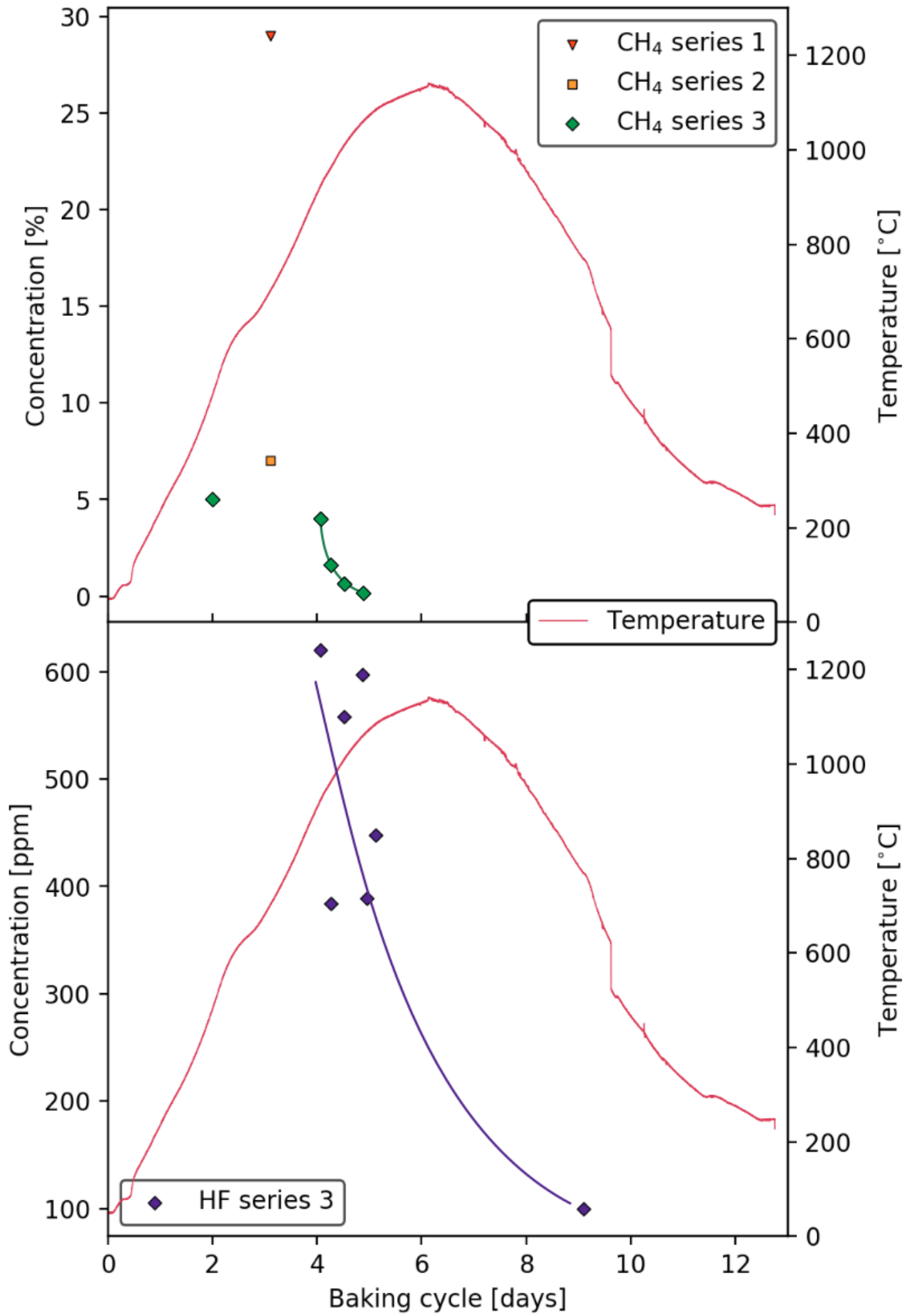
122 Figure 2: Concentration of CO and CO₂ from series 1 during the baking cycle. The corresponding
 123 temperature is also shown.

124 Concentrations of CO and CO₂ from all three series are presented in Figure 3. The figure gives an
 125 overview of the development of CO and CO₂ concentration during a baking cycle. Here, the aspects
 126 addressed in series 1 are emphasized by the results from series 2 and 3. The temperature cycle is fairly
 127 similar for all series, and the temperature curve from series 1 is used for all three data sets. During
 128 heating of the anodes, the FTIR data shows that the pit atmosphere is to a large extent dominated by
 129 CO₂, peaking at 12 - 13 %. As the temperature increases, the CO₂ concentration is reduced while CO
 130 increases to 15 % at the most. The measured levels are a clear indication that much of the CO and
 131 CO₂ origins from packing coke reacting with oxygen in the air. During the highest baking
 132 temperature, CO remains the dominating specie, before CO₂ again starts to appear at ~800 °C during
 133 cooling. In the last part of the baking cycle, it is clear that CO concentration goes down as CO₂
 134 becomes the dominating reaction product in the pit, peaking at 15-16 %. The ratio between CO and
 135 CO₂ concentration is shown in the lower part of Figure 3, emphasizing the abovementioned shifts in
 136 concentrations. In addition to FTIR measurements, some regions of series 3 were also covered by the
 137 gas chromatography (GC) measurements. At ~930 °C during the heating cycle, hydrogen was
 138 estimated to near 80 %, while N₂ and O₂ were estimated to 16 % and 3 %, respectively. The
 139 instrument was calibrated to measure H₂ up to 20 %, and a linear extrapolation was used outside this
 140 range. The estimation demonstrates that the H₂ level was significantly higher than 20 %, but it was
 141 difficult to determine the exact level. A longer period was sampled during the cooling period of series
 142 3. Between ~890 °C and ~850 °C, the H₂ estimate declined from 7500 ppm to 5800 ppm, CO₂
 143 increased from 7.5 % to 9.5 %, O₂ was stable at 3.1 % and N₂ increased from 78 % to 80 %.



145 Figure 3: Concentration of CO and CO₂ from series 1, 2 and 3. The lower part of the figure shows the
146 ratio between CO and CO₂, illustrating the shift in the dominating specie from CO (high temperature)
147 to CO₂ (low temperature). The temperature profile plotted for series 2 applies for all series.

148 In addition to the shifts in CO and CO₂ concentrations during the cycle, the pit gas atmosphere at
149 three stages in the cycle is presented in Table 1, illustrating the variation in pit gas composition. Other
150 observed gaseous compounds are included to give a broader overview of the gas composition. At
151 700 °C during heating, the CH₄ level is measured to 29 % in series 1 and 7 % in series 2. The top part
152 of Figure 4 summarizes the overall development of CH₄ based on the available data. A peak in CH₄
153 concentration is present in the range of 400 to 850 °C, which diminishes during further heating. The
154 height of the peak is varying between the series. HF was measured in significant concentrations at
155 ~1100 °C in series 3, presented in the lower part of Figure 4. When comparing the concentrations in
156 Table 1 at 700 °C during heating and cooling, there are some notable differences. Firstly, the high
157 concentration of CH₄ measured during heating is not present towards the end of the cycle. Secondly,
158 the level of CO₂ is much higher and more stable in the last part of the cycle, while varying more
159 during heating. At 700 °C during heating, the CO₂ concentration in series 1 and 2 is measured to
160 0.15 % and 2 %, as shown in Table 1. At the same temperature during cooling, the CO₂ level is
161 measured in the range from 8 % to 12.9 %.



162

163 Figure 4: Concentrations data of CH₄ and HF. Both compounds are mostly present during the first part
 164 of the baking cycle.

165 Table 1: Concentration data from series 1, 2 and 3, covering three periods of the baking cycle. For
 166 NH₃ linear extrapolation from 0.1 % was performed. The spectral line for C₆H₆ was compared to a
 167 0.1 % library spectrum, which indicated a concentration higher than 0.1 %. Exact quantification was
 168 however difficult due to overlapping signals from other species present in the gas.

	~700 °C (heating)		~1150 °C (max temp)			~700 °C (cooling)		
	S1	S2	S1	S2	S3	S1	S2	S3
CO [%]	1.5	1.1	2.9	5	5.3	1.5	0.18	1.1
CO ₂ [%]	0.15	2	175 ppm	0.6	0.1	8	12.5	12.9
H ₂ O [%]	2.2	1	2.0	6.1	0.5	0.6	6.3	0.7
CH ₄ [%]	29	7	0.1		285 ppm			
NH ₃ [%]	~ 1	~ 0.1						
C ₆ H ₆ [%]	> 0.1							
HF [ppm]					400-597			

169

170 During the first 24 hours of the baking cycle, water was extracted from the condensation vessel. The
 171 average condensation rate of water was measured to 0.19 kg water per hour. Based on the pressure
 172 difference over the FTIR nozzle during the 24 hours of water condensation, the average gas flow was
 173 estimated to 0.5 – 1.0 L per minute. With the estimated gas flow, the average water content of the pit
 174 gas was 3.2-6.5 g per L gas. The pit temperature increased from 75 °C to 330 °C over the sampling
 175 period, and the condensation rate was fairly constant over that temperature range.

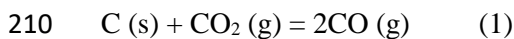
176 In the temperature range from 400 to 800 °C during heating, pitch residues were observed to
 177 accumulate in the condensation vessel. A brown/yellow, sticky condensate was found in the bottom of
 178 the vessel, illustrating the good control of condensation. If similar compounds had accumulated in the
 179 narrow parts of the piping or in the filter, the experiment would suffer greatly from reduced flow
 180 through the equipment. Some lighter volatiles escaped the vessel and were captured in the filter
 181 material instead, discoloring the filter material. As the temperature increased beyond 800 °C, the level
 182 of condensation diminished and the gas became cleaner with respect to pitch residues.

183 In addition to the data presented above, several other compounds were also detected during the
 184 experiments. During the heating period of series 1 and 2, NH₃ was measured to 0.1 - 1 %. In the same
 185 period of the baking cycle, ~200 ppm HCN was detected in series 3. Details concerning the
 186 hydrocarbons showed that both ethane and propane were present, but methane being the dominating
 187 specie of the three. 300 ppm of HF was detected in series 2 at 400 °C during temperature decrease.
 188 Finally, sulfur compounds were detected in the last part of the baking cycle in series 3. At 625 °C, a
 189 distinct shift from COS to SO₂ was measured. Extrapolation of library data from 200 ppm indicated a
 190 COS concentration of ~700 ppm. SO₂ was measured to maximum 2500 ppm.

191 4. Discussion

192 4.1 The pit environment

193 The gas composition in the anode baking furnace, measured in this study, varied greatly during the
194 course of a baking cycle. This expected variation is mainly affected by two factors; the temperature
195 cycle and the baking processes going on in the anodes. The gas composition at 700 °C during heating
196 and cooling, presented in Table 1, shows a high level of CH₄ during heating, while CO₂ is dominating
197 during cooling. The temperature in the packing coke is measured to 700 °C in both cases, but the
198 different gas atmospheres demonstrate that the chemical and overall thermal conditions are far from
199 being equal during heating and cooling. During heating, the coal tar pitch in the anodes are
200 decomposing, creating an atmosphere of volatile hydrocarbons, including CH₄. As the temperature
201 increases, and the pitch decomposition process ceases and the concentration of CH₄ diminishes, as
202 presented in Figure 4. This is also in accordance with the low thermodynamic stability of CH₄ at
203 elevated temperatures^[13]. At 700 °C during cooling, the pitch decomposition is no longer a dominating
204 factor. The gas composition mainly consists of CO₂ at this stage, after a dramatic decrease in CO
205 during cooling from maximum baking temperature. This is in accordance with the expected
206 thermodynamic behavior. Due to the lower pressure inside the pit compared to the outside, air is
207 entering the furnace through the packing coke. Oxygen is thus reacting with the packing coke
208 producing CO or CO₂. The overall thermodynamic equilibrium between CO and CO₂, with solid
209 carbon present, is assumed to be governed by the Boudouard reaction (Reaction 1):



211 This reaction becomes spontaneous above 700 °C. Figure 3 show the time series of all three series,
212 where the reduction in CO upon cooling is clearly present. With solid carbon present, Equation 1 will
213 be the governing reaction between CO and CO₂ at equilibrium, and the ratio $(p_{\text{CO}})^2/p_{\text{CO}_2}$ describes the
214 relation between the equilibrium partial pressures of CO and CO₂.

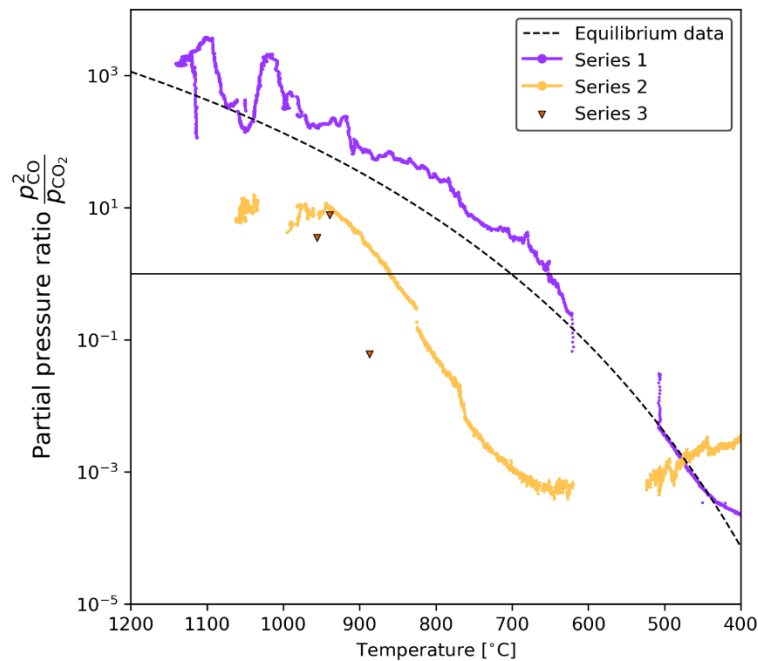
215 The ratio between $(p_{\text{CO}})^2$ and p_{CO_2} of the experimental data from series 1, 2 and 3 are presented in
216 Figure 5, comparing the experimental data to the same ratio based on equilibrium data. The ratios are
217 plotted as a function of measured temperature in order to more easily follow the evolution during
218 cooling in the last part of the baking cycle. When comparing the experimental data to the equilibrium
219 data, it is possible to evaluate the degree of equilibrium in the pit gas in each series. In general, the
220 experimental data is in good accordance with the equilibrium ratio, both with respect to the level and
221 the temperature dependence. The data from series 1 is following the equilibrium ratio especially well,
222 and the gas composition in series 1 during cooling can thus be assumed to roughly be in equilibrium.
223 The results from series 2 and 3 also indicate a good correspondence with the equilibrium ratio, but not
224 to the same degree as for series 1. The Boudouard reaction can thus be regarded as a good model for
225 describing the pit atmosphere in this part of the cycle.

226 The pit gas composition is in general showing similar trends in all three series, where the same main
227 gas components are observed, and their concentration profile through the baking cycle are

228 comparable. There are however some quantitative discrepancies from series to series. These variations
229 are mostly related to the amount of gas measured in various parts of the baking cycle, and could be
230 due to both experimental challenges and real variations from one baking cycle to another. The
231 absolute value of CH₄ during the heating period (presented in Figure 4) is for example varying from
232 one series to the next. Based on this work, it is therefore difficult to determine the accurate
233 concentration of the various gas components throughout the baking cycle. However, based on this
234 study we have been able to establish the gas component present in the baking furnace and how the
235 concentration of these species vary qualitatively through the baking cycle.

236 The temperature probe is positioned in the packing coke between the anodes and flue wall. The actual
237 temperature in the flue wall and inside the anodes are hence not necessarily the same as the
238 temperature measured in these experiments. A study modelling the flow of gas in the flue walls report
239 on potential thermal gradients across the flue walls in the range of 50 - 100 °C [14]. In addition, the
240 heating rate of the anodes is assumed to create a thermal gradient from the center of the anode and
241 outwards during heating, with the opposite direction during cooling. The temperature in the center of
242 the anode is thus not the same as the temperature measured by the thermocouple in the packing coke.
243 During heating, most of the processes occurring within the anodes (evaporation and cracking of pitch)
244 are occurring at a lower temperature than measured by the probe. Due to the delay in heat transport
245 from the surface to the center of the anode, the actual anode temperature will always be lower than
246 measured in the packing coke during heating. Similarly, as the furnace is cooled in the last part of the
247 baking cycle, the anode temperature will be higher compared to the measured temperature in the
248 packing coke. The measured pit gas composition is also very dependent on reaction kinetics,
249 especially in the first part of the cycle when the pitch is evaporating and cracking. The thermal
250 gradients and reaction kinetics do therefore result in variation in the evolution of the pit atmosphere
251 from one backing cycle to another, particularly during heating. We therefore expect some variation in
252 the pit atmosphere during heating and a different atmosphere during cooling compared to heating. The
253 GC data from series 3 complements the overall FTIR measurements. At 930 °C during heating, the H₂
254 level was estimated to ~80 %. This estimate is based on a linear extrapolation from the upper limit of
255 the calibration range at 20 %. The H₂ concentration is therefore not accurately determined, and should
256 not be used for quantitative evaluation. There is however no doubt that the H₂ concentration is very
257 high in this part of the cycle. The N₂ estimate (16 %) and O₂ estimate (3 %) demonstrate a significant
258 dilution of incoming air, most likely originating from the formation of H₂. The nitrogen to oxygen
259 ratio in the pit (5.3) is higher compared to air (~4), resulting from oxygen consumption by reaction
260 with the packing coke. The reaction between O₂ and the packing coke, forming CO and/or CO₂, will
261 also contribute to dilution of nitrogen and oxygen. Between ~890 °C and ~850 °C during cooling, the
262 GC measurements showed a distinct different pit gas concentration. The nitrogen level is now
263 approximately the same as in air, while the oxygen concentration is estimated to 3.1 %. The high

264 nitrogen level demonstrate that the dilution of incoming air by formation of gases in the pit is low.
 265 The low oxygen level is reflecting the reaction of oxygen with carbon. The draft in the furnace, i.e.
 266 the reduced pressure in the flue gas, causing air to flow into the furnace, is lower towards the end of
 267 the baking cycle. This results in less air flow and more time for the oxygen to react in this part of the
 268 cycle. An oxygen concentration of 3.1 % is, however, higher than expected from the reaction kinetics
 269 (air burn) at these temperatures. The GC coverage of these experiments are low compared to the FTIR
 270 measurements, and some caution is therefore advised when interpreting the GC results.



271

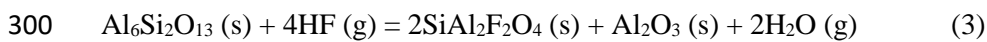
272 Figure 5: The ratio between $(p_{CO})^2$ and p_{CO_2} for series 1, 2 and 3, in addition to equilibrium data,
 273 plotted as a function of temperature. The experimental data is in good accordance with the
 274 equilibrium data.

275 4.2 Implications of water condensation

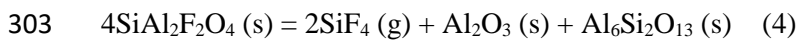
276 Water was measured in significant quantities during the first part of the baking period. The average
 277 condensation rate of water during the first 24 hours was 0.19 kg/hour, corresponding to a pit gas
 278 humidity of 3.2 – 6.5 g/L. The high level of water in the pit causes dramatic changes to the chemical
 279 environment in the pit, especially affecting the volatility of traces of fluorides from recycled anode
 280 butts. Thermodynamic calculations carried out on cryolite, representing the electrolyte, and water,
 281 show an onset of fluoride volatility at a lower temperature compared to a system with dry cryolite^[15].
 282 With no water present, cryolite decomposes into NaF and NaAlF₄ above 1000 °C^[7,15]. When cryolite
 283 is heated in an atmosphere containing water, HF volatility is becoming significant above 800 °C,
 284 following Equation 2.



286 The presence of water in the pit is thus lowering the onset temperature for fluoride volatility, in
287 addition to favor the formation of HF over NaF/NaAlF₄^[15]. The measured level of HF in series 3 is
288 presented in the lower part of Figure 4. Between 900 and 1100 °C during heating, HF was measured
289 to 400 – 600 ppm. These values are given by the instrument built-in model and are most likely an
290 underestimate the actual HF concentration. A manual evaluation of the HF signal was attempted,
291 where the experimental signal was compared to calibration data for various concentrations. Due to the
292 complexness of the experimental signal and the lack of easily interpreted data, it was found difficult to
293 give accurate values for the HF concentration. The data from the instrument built-in model was
294 therefore decided to be used. However, based on overall signal from the FTIR, the true HF
295 concentration is proposed up to 1500 – 2000 ppm. Regardless of the actual HF level, the important
296 observation is that HF is present in the furnace in significant amounts. A thermodynamic assessment
297 has addressed the effect of HF on aluminosilicate refractories during a baking cycle^[15]. Mullite
298 (Al₆Si₂O₁₃), a major phase in many aluminosilicate materials, reacts with HF to form SiAl₂F₂O₄ at
299 moderate temperatures in accordance to Equation 3:



301 SiAl₂F₂O₄ is however not thermally stable and will decompose above ~1100 °C as described in
302 Equation 4.



304 Through the reaction path described here, fluorine ends up as gaseous SiF₄ leaving the furnace
305 through the off-gas. Based on these considerations, it is thus not expected to find fluorides in autopsy
306 samples of refractory linings. The calculations are also addressing the tendency for traces of the
307 electrolyte in the green anode to react with water before decomposing into NaF and NaAlF₄^[15]. Water
308 is thus “cleaning” the green anodes for electrolyte. A recent study of spent refractory lining has
309 reported very low levels of sodium in the samples, and related this to low levels of electrolyte in the
310 green anodes^[8]. However, with the current observations of water and HF in the pit, some electrolyte
311 must be present in the green anodes, reacting with water before reaching its decomposition
312 temperature. Several studies on spent refractory lining reports regions or layers of SiO₂ depletion^{[8–}
313 ^{10,16]}. As described in Equations 3 and 4, HF reacts with the lining to form a condensed fluoride phase,
314 which, when heated above 1100 °C, forms gaseous SiF₄ and depletes the lining of silicon. This
315 reaction path could explain the SiO₂ depletion observed in the spent lining in other studies^[8–10,16].

316 During production of the green anodes, extensive use of water cooling is applied after forming in
317 order to regain mechanical stability prior to storage. The anodes are immersed into a water basin and
318 kept there for ~2 hours, while the anodes are cooled and water is absorbed into the open porosity. The
319 Mettler softening point of pitch is usually 110 – 120 °C^[17], and the anodes must be cooled below this
320 temperature to avoid creep during storage. To reduce the amount of water in the green anodes, it could

321 therefore be interesting to investigate the water content in relation to soaking time. If the anodes are
322 removed from the water basin at e.g. 80 °C, there is still enough residual heat in the anodes to increase
323 the evaporation of water during storage.

324 **4.3 Evaluation of the experimental method**

325 *In situ* measurements of pit gas composition has proven to be a challenging, but rewarding exercise.
326 Especially with respect to the setup design and the obstacles with measuring pit gas continuously
327 during the whole cycle. The degree of pitch residue condensation was much higher than first
328 expected, and the construction of a condensation vessel and increase in pipe diameters were direct
329 consequences of that observation. With the condensation vessel in place for series 2, it became
330 possible to run the experiment during the heating period, which resulted in large amounts of water in
331 the condensation vessel. The high condensation rate measured during the first 24 hours of the baking
332 cycle was not expected, but seen in light of the extensive use of water cooling, not surprising. The
333 pressure drop over the filter cylinder increased when the XAD-2 was wetted, and the filter material
334 had to be changed regularly during the humid period of the cycle. Series 2 was carried out in the
335 middle of December with an outside temperature below -20 °C. This caused the outlet tube from the
336 FTIR to freeze due to humidity in the gas, and several discontinuities occurring in the measurements.
337 Given these challenges, combined with the long duration of the baking cycle, measurements of pit gas
338 during anode baking has not been a trivial experimental exercise. The results have, on the other hand,
339 given valuable insight in the development of the pit gas atmosphere during the anode baking process.

340 Spectral analysis from the experiments have in some cases been challenging. Especially in the first
341 part of the baking cycle, where the level of pitch residues high and the raw spectra were a mixture of
342 partly overlapping signals. The setup was not designed for controlled dilution prior to the FTIR
343 analysis, resulting in the signal exceeding the detection limit of the instrument. The main peak of CO₂
344 (~2350 cm⁻¹) is reaching the detector limit at ~1 %, hence secondary peaks had to be used in the
345 analysis. The secondary peaks are however interfering with the IR response from water, making
346 accurate quantitative analysis above moderate concentrations in humid atmospheres difficult. The
347 same was experienced with HF in series 3, where the underestimated values from the model were
348 used due to difficulties finding frequencies without interference for manual evaluations. That being
349 said, the overall experimental results give a good indications of the dominating compounds and the
350 trends in gas compositions over the course of a baking cycle.

351 The data presented in this study is based on three experimental series of pit atmosphere, conducted
352 over the course of 15 months. The measurement were carried out in different sections of the baking
353 furnace, in pits of varying age. The three series cover various parts of the baking cycle, with varying
354 degree of overlap. The spread in sampling periods is due to the experimental design and unexpected
355 difficulties during the measurements. Most of the pitch components are found to vaporize during the

356 first part of the heating cycle (from 400 °C to 800 °C), constituting a critical period in terms of
357 potential pipe or filter blockage. This period was thus omitted in some of the series in order to
358 maintain an open system for the rest of the experiment. HF was measured in considerable
359 concentration during the third series, constituting a significant threat to the silica-based optics in the
360 FTIR instrument. Some parts of the third series are therefore shorter measurements spread out instead
361 of continuous measurements.

362 **5. Conclusion**

363 *In situ* measurements of pit gas atmosphere during anode baking were successfully performed by
364 FTIR spectroscopy. The experiments resulted in valuable insight in the development of pit
365 atmosphere as a function of baking time and temperature. Time series of CO and CO₂ showed that
366 CO₂ is the dominating specie at moderate temperatures, while CO takes over above ~700 °C.
367 Condensation of water at an average rate of 0.19 L/hour was measured the first 24 hours of the baking
368 cycle. Between 400 °C and 800 °C during heating, large concentrations of CH₄ was present,
369 originating from the decomposition of pitch in the anodes. At ~1100 °C during heating, significant
370 levels of HF was detected, expected to come from the reaction between cryolite in the anodes and
371 water. HF have a destabilizing effect on the refractory oxides, and could serve as an explanation for
372 the earlier reported SiO₂ depletion.

373 **Acknowledgements**

374 Financial support from the Norwegian Research Council and the partners Hydro Aluminium, Alcoa,
375 Elkem Carbon and Skamol through the project "Reactivity of Carbon and Refractory Materials used
376 in metal production technology" (CaRMa) is acknowledged. Technical support from Roger Moen,
377 Morten Aanvik, Martin Aufles, Mona Aufles Hines and the other staff at Alcoa Mosjøen during the
378 measuring campaigns is acknowledged and highly appreciated.

379

380 **References**

- 381 1 E.H.M. Moors: *J. Clean. Prod.*, 2006, vol. 14, pp. 1121–38.
- 382 2 H.-G. Schwarz, S. Briem, and P. Zapp: *Energy*, 2001, vol. 26, pp. 775–95.
- 383 3 F. Becker and F. Goede: *Alum. Int. J.*, 2006, pp. 1–15.
- 384 4 P. Prigent and M.L. Bouchetou: *Interceram*, 2009, vol. 58, pp. 202–9.
- 385 5 P. Prigent and M.L. Bouchetou: *Interceram*, 2009, vol. 58, pp. 121–6.
- 386 6 T. Brandvik, A.P. Ratvik, Z. Wang, and T. Grande: *Light Met.*, 2017, pp. 1281–8.
- 387 7 T. Brandvik, A.P. Ratvik, and T. Grande: Proceedings of the 34th International ICSOBA

- 388 Conference 2016.
- 389 8 T. Brandvik, Z. Wang, A.P. Ratvik, and T. Grande: *Int. J. Appl. Ceram. Technol.*,
390 DOI:<https://doi.org/10.1111/ijac.13108>.
- 391 9 F. Brunk: *Light Met.*, 1995, pp. 641–6.
- 392 10 N. Oumarou, D. Kocaefe, and Y. Kocaefe: *Ceram. Int.*, DOI:10.1016/j.ceramint.2016.08.178.
- 393 11 T.A. Aarhaug, T. Brandvik, O.S. Kjos, H. Gaertner, and A.P. Ratvik: in *Light Metals*, 2018,
394 pp. 1379–85.
- 395 12 T.A. Aarhaug, T. Brandvik, H. Gaertner, A.P. Ratvik, and O.S. Kjos: in *AASTC*, 2018.
- 396 13 D. Trommer, D. Hirsch, and A. Steinfeld: *Int. J. Hydrogen Energy*, 2004, vol. 29, pp. 627–33.
- 397 14 F. Grégoire and L. Gosselin: *Int. J. Therm. Sci.*, 2018, vol. 129, pp. 532–44.
- 398 15 T. Brandvik, A.P. Ratvik, and T. Grande: Travaux 47, Proceedings of the 36th International
399 ICSOBA Conference, 2018, pp. 555-562.
- 400 16 Z. Wang, S. Rørvik, A.P. Ratvik, and T. Grande: *Light Met.*, 2017, pp. 1265–74.
- 401 17 C. Sommerseth, R. Thorne, A. Ratvik, E. Sandnes, H. Linga, L. Lossius, and A. Svensson:
402 *Metals (Basel)*, 2017, vol. 7, p. 74.

403

404

405

406

407

408

409 List of figures

410 Figure 1: Overview of the experimental setup used in the second and third measurement campaigns.
411 The Kanthal probe consists of two concentrically mounted pipes. The inner diameter, outer diameter
412 and length are 20.9 mm, 36.7 mm and 4200 mm (inner pipe), and 34 mm, 40 mm and 4500 mm (outer
413 pipe), respectively.

414 Figure 2: Concentration of CO and CO₂ from series 1 during the baking cycle. The corresponding
415 temperature is also shown.

416 Figure 3: Concentration of CO and CO₂ from series 1, 2 and 3. The lower part of the figure shows the
 417 ratio between CO and CO₂, illustrating the shift in the dominating specie from CO (high temperature)
 418 to CO₂ (low temperature). The temperature profile plotted for series 2 applies for all series.

419 Figure 4: Concentrations data of CH₄ and HF. Both compounds are mostly present during the first part
 420 of the baking cycle.

421 Figure 5: The ratio between ratio $(p_{CO})^2$ and p_{CO_2} for series 1, 2 and 3, in addition to equilibrium data,
 422 plotted as a function of temperature. The experimental data is in good accordance with the
 423 equilibrium data.

424

425 List of tables

426 Table 1: Concentration data from series 1, 2 and 3, covering three periods of the baking cycle. For
 427 NH₃ linear extrapolation from 0.1 % was performed. The spectral line for C₆H₆ was compared to a
 428 0.1 % library spectrum, which indicated a concentration higher than 0.1 %. Exact quantification was
 429 however difficult due to overlapping signals from other species present in the gas.

430

	~700 °C (heating)		~1150 °C (max temp)			~700 °C (cooling)		
	S1	S2	S1	S2	S3	S1	S2	S3
CO [%]	1.5	1.1	2.9	5	5.3	1.5	0.18	1.1
CO ₂ [%]	0.15	2	175 ppm	0.6	0.1	8	12.5	12.9
H ₂ O [%]	2.2	1	2.0	6.1	0.5	0.6	6.3	0.7
CH ₄ [%]	29	7	0.1		285 ppm			
NH ₃ [%]	~ 1	~ 0.1						
C ₆ H ₆ [%]	> 0.1							
HF [ppm]					400-597			

431